Article

A Highly-Efficient Electrochemiluminescent Ag Nanoclusters/TiO2 Nanomaterials as Signal Probe for Ferrocene-Driven Light Switch Bioanalysis

Ying Zhou, Haijun Wang, Ying Zhuo, Yaqin Chai, and Ruo Yuan

Anal. Chem., **Just Accepted Manuscript** • DOI: 10.1021/acs.analchem.7b00090 • Publication Date (Web): 22 Feb 2017

A Highly-Efficient Electrochemiluminescent Ag Nanoclusters/TiO_2 Nanomaterials as Signal Probe for Ferrocene-Driven Light Switch Bioanalysis

Ying Zhou, Haijun Wang, Ying Zhuo, Yaqin Chai*, Ruo Yuan*

Key Laboratory of Luminescent and Real-Time Analytical Chemistry (Southwest University), Ministry of Education, College of Chemistry and Chemical Engineering, Southwest University, Chongqing 400715, PR China

[1] *Corresponding authors at: Tel.: +86 23 68252277, fax: +86 23 68253172.
E-mail addresses: yuanruo@swu.edu.cn (R. Yuan); yqchai@swu.edu.cn (Y. Q. Chai).

ABSTRACT:

In this work, a ferrocene (Fc)-driven light switch biosensor for ultrasensitive detection of amyloid-β (Aβ) was designed by utilizing the highly-efficient electrochemiluminescent nanomaterials of Ag NCs/TiO_2 nanoflowers (NFs) as signal labels. Through combining the TiO_2 NFs as the co-reaction accelerator and dissolved O_2 as the intrinsic co-reactant to in suit generate strong oxidizing intermediate radical $OH^{\bullet}$, the electrochemiluminescence (ECL) of Ag NCs on the TiO_2 NFs surface could be significantly promoted in comparion with that of pure Ag NCs in solution. Further, Fc-labeled DNA as ECL quenching probe was introduced to dramatically restrain the ECL emission of nanomaterials, which facilitated to improve the sensitivity of the prepared biosensor to a large extent. Surprisingly, tiny amounts of target protein could be recognized by the immunoreaction-induced DNA nanostructure for outputting numerous secondary target DNAs, which further triggered the release of Fc to recover the ECL signal, realizing the ultrasensitive detection of target. As a result, this developed assay for Aβ detection demonstrated excellent sensitivity with linear range from 50 fg/mL to 500 ng/mL and limit of detection down to 32 fg/mL, which opened up a new research direction for ultrasensitive ECL bioanalysis based metal NCs.

KEYWORDS: highly-efficient luminescent efficiency; Ag NCs-TiO_2 NFs nanomaterials; ultrasensitive ECL bioanalysis; ferrocene driven light switch

INTRODUCTION:

With the size approaching the electron Fermi wavelength, the spatial confinement of free electrons in metal nanoclusters (NCs) generates discrete and size-tunable electronic transition, leading to molecular-scale properties such as electrochemiluminescence (ECL). [1-3] Therefore, metal NCs process a set of superior features, such as low toxicity and ease of labeling, establishing them as a new class of

ECL label for biological applications, especially for biosensing and bioimaging. [4-6] Currently, many research efforts have been made to improve their luminous intensity by adding the coreactant into working soultion. Ding et al. explored ECL properties of Au NCs using the benzoyl peroxide as the coreactant. [7] Zhu's group developed an Au NCs-based ECL sensor for the detection of dopamine with the catalyst of $S_2O_8^{2-}$. [8] However, the luminous intensity of metal NCs remained too low to achieve sensitive biodetection for the lack of enough ECL luminophore, which because the ultarsmall dimension of metal NCs was adverse to further separation, purification and immobilization. In our previous work, we in situ synthesized plentiful Ag NCs on the electrode as ECL signal probes for sensitive detection of microRNA based on the high affinity of silver ions with cytosine-rich DNA.[9] The work achieved immobilization of Ag NCs, but still relied on additional coreactant to improve ECL performance, which suffered from the problems of operational complexity. Therefore, it is challenging to seek a high-efficient immobilization substrate of Ag NCs for significantly promoting luminescence without the help of additional coreactant and then broaden its application into the ultrasensitive biosensors.

Reactive oxygen species (ROS) [10, 11], including superoxide ($O_2^{\bullet-}$), singlet oxygen (O_2^1) and hydroxyl radical ($OH^{\bullet}$), act as important activated molecules that can be generated in the decomposition process of $S_2O_8^{2-}$, H_2O_2 or dissolved oxygen, which play key roles in the ECL performance of metal NCs. [12, 13] But usually, the concentration of dissolved oxygen in the testing solution is so low that cannot offer effective signal amplification. Titanium dioxide (TiO_2) as a kind of prominent metal oxide semiconductors, exhibiting the band gap-depended catalytic properties, has been widely researched for many decades, which can aggregate dissolved oxygen on the interface and reduce oxygen to ROS. [14, 15] While TiO_2 possesses flower-like

nanostructure (nanoflowers), their catalytic performance can be further improved because more effective area contact with more dissolved O_2. Herein, Ag NCs were in situ generated on the surface of bovine serum albumin (BSA) functionalized TiO_2 nanoflowers (TiO_2 NFs), in which BSA as stabilizing agent provided abundant binding sites to potentially bind and reduce Ag ions. [16] (The pure TiO_2 with a large number of the irregular branchs had a flower-like nanostructure and shown in the Figure S2.) Notably, TiO_2 NFs effectively promoted the reduction of dissolved O_2 to generate the strong oxidizing intermediate radical $OH^{\bullet}$, which could in suit react with Ag NCs to produce excited state species Ag NCs* for emitting ECL remarkably. Meanwhile, the ECL of novel nanomaterials could be prominently quenched by ferrocene (Fc) which could efficiently consume ROS, [17, 18] thus afforded a sensitive quantitative method in biosensor applications.

Up to now, double-antibody sandwich based protein recognition is a common approach in the quantitative immunological assay. [19, 20] However, this technique is difficult to improve the sensitivity due to absence of intrinsic amplification strategy. The exquisite sequence predictability and interaction specificity made various DNA-based amplification strategies successfully apply to bioanalysis [21- 23]. Inspired by these, the DNA nanostructure [24] was employed by DNA probes labeled antibodies as affinity ligands, immune sandwich reaction as switch and Exo III cleavage as drive so that it could transform tiny amounts of target protein to numerous secondary target DNAs, offering the advantages of high specificity, excellent sensitivity, and precise control in widespread target protein detection application. Alzheimer's disease (AD) as a progressive irreversible neurological disorder had extremely threated the human's health seriously and reduced quality of life. [25] It has been reported that amyloid-β (Aβ) protein was proved as the pathogenesis of AD. Therefore, the identification and

quantification of Aβ during early stages of AD progress is of extreme importance. [26] Herein, the immunoreaction-induced DNA nanostructure was employed for ultrasensitive detection of Aβ.

To take advantage of the remarkable ECL intensity of Ag NCs-TiO_2 NFs and high quenching efficiency of Fc, the ultrasensitive biosensor achieved Aβ quantitative test by controlling luminescence switch of Ag NCs in the on-off-on platform, termed as Fc driven light switch sensor. As shown in Scheme 1, Ag NCs-TiO_2 NFs was immobilized onto glassy carbon electrode (GCE) to obtain the strong ECL signal as "switch on" state, which also acted as the active interface to immobilize thiol-modified capture DNA (P_1) *via* Ag-N or Ag-S covalent bond. Subsequently, the "switch off" state was obversed based on the quenching effect of Fc towards Ag NCs, when the Fc-labeled assistant probes (P_2) triggered the DNA hybridization reaction with P_1. Then, the exposed part of P_2 as an initiator could hybridize with secondary target DNA (T) to trigger Exo III cleavage process, accompanied by releasing Fc and achieving the second "switch on" state. Inspired by the intellectual scientific interests, the preparation method of highly-efficient electrochemiluminescent signal probe based Ag NCs not only expanded the application of metal NCs in ultrasensitive biodetection, but opened up a new research direction for the development of biosensor.

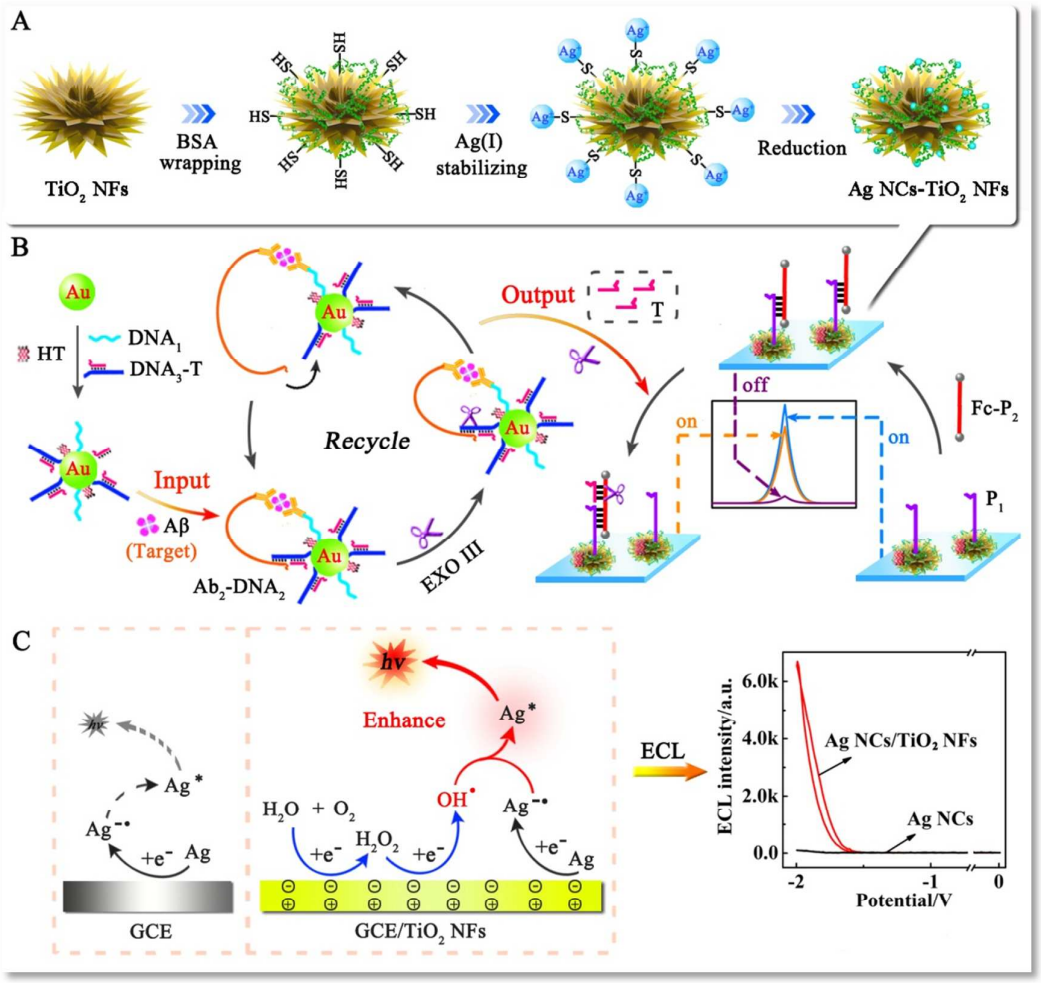

Scheme 1. The schematic diagrams shown the preparation of Ag NCs-TiO_2 NFs (A), ultrasensitive detection of Aβ by combining immunoreaction-induced DNA nanostructure with Fc-driven light switch bidetection (B), and possible ECL emitting mechanism of Ag NCs-TiO_2 NFs (C).

EXPERIMENTAL SECTION

Preparation of TiO_2 NFs. TiO_2 NFs was synthesized by a general hydrothermal method. Titanium potassium oxalate (0.05 M) was diluted in 8.0 mL of deionized water in a vial, following by adding H_2O_2 (8.0 mL) solution with continuous magnetic stirring for 30 min. The molar rate of titanium and H_2O_2 was 1:1. Then, the pH of the solution was adjusted to 4 with HCl solution, while the color of the solution rapidly changed from bright yellow to dark red. And then, this mixed solution was put into an autoclave and maintained warm at 150 ºC for 1 h. Finally, the obtained TiO_2 NFs were

collected by centrifugation and dispersed in 2 mL deionized water for further use.

Preparation of Ag NCs-TiO_2 NFs. In a typical experiment, the 2 mL prepared TiO_2 NFs were surface-chemically modified by 1 mL 3% bovine serum albumin (BSA) to obtain the -SH or -NH_2 groups functionalized TiO_2 NFs. After that, the mixture was centrifugated and washed by deionized water to clean up uncombined BSA. Next, 2 mL BSA functionalized TiO_2 NFs were successively treated with 1 mL 10 mM silver nitrate under vigorous stirring. Two minutes later, NaOH solution (0.2 mL, 1 M) was introduced, and the mixture was reacted at 37 ºC for 12 h. The nanomaterials was successfully obtained when the color of the solution changed from milk white to light yellow. After the process of centrifugation and clean, the resultant products were stored at 4 ° C for further use.

Preparation of Ab_2-DNA_2. First, the carboxyl of DNA_2 (50 μL, 20 μM) was activated in 140 μL PBS (pH 7.4) containing 10 mg NHS and 40 mg EDC for 2 h at 4 ºC. Second, 10 μL Ab_2 was added into the above-mentioned solution and reacted for 4 h to form amido bond between DNA_2 and Ab_2. After the solution was ultrafiltrated by a 20000 MW dialysis membrane, the Ab_2-conjugated DNA_2 (Ab_2-DNA_2) were resuspended in 100 μL PBS (pH 7.4). The Figure S1 demonstrated the coupling efficiency of the product by the polyacrylamide gel electrophoresis.

Construction of Immunoreaction-Induced DNA Nanostructure. The nanostructure was prepared by reported technique with certain modifications [24]. The AuNPs were functionalized with 10 μL of 2.0 μM DNA_1 and 10 μL of 20 μM DNA_3 in the 80 μL Tris-HCl buffer at room temperature overnight. Specifically, 20 mg EDC, 5 mg NHS and1 mM HT were respectively added into the above-mentioned solution to activate the carboxyl group of DNA_1 and block nonspecific binding sites of AuNPs. And then secondary target DNA (T, 10 μL, 2.0 μM) were hybridized on the DNA_3,

and 10 μL Ab_1 were linked with DNA_1 *via* amidation reaction using same experimental procedure. Then, separating nonhybridized DNA_1 and nonreaction Ab_1, 20 μL DNA-functionalized AuNP soulation was mixed with 20 μL of DNA_2-Ab_2 and various concentrations Aβ solution at 37 ºC for 2h to activate the nanostructure. Upon the addition of 20 μL 2.0 U mL^{-1} Exo III, DNA_3 was digested to release DNA T. Finally, solutions containing various concentrations of DNA T and remanent Exo III could be collected by centrifugation, and stored at 4 ºC for further use.

Fabrication of the ECL Biosensor. Before modification, the GCE (Φ = 4 mm) was continuously polished with 0.3 and 0.05 mm alumina slurry and then cleared thoroughly with deionized water in the ultrasonic apparatus. At first, 5.0 μL of Ag NCs-TiO_2 NFs solution was directly dropped and modified onto the clear electrode surface due to the great film-forming property of TiO_2. After drying, 5.0 μL of 2.0 μM thiol-modified P_1 was incubated on the electrode *via* Ag-N bond for 6 h at 4 ºC. Following that, 5.0 μL of Fc-labeled P_2 (2.0 μM) was dropped onto the GCE for 12 h at room temperature to form the P_1/P_2 duplex for immobilizing Fc on the above modified electrode, which had the remarkable quenching toward Ag NCs ECL system. After blocking nonspecific binding sites, 10 μL of a mixture containing different concentrations of outputted T and remanent Exo III were dropped onto the modified electrode and incubated for 1 h at room temperature. Ultimately, preceding Exo III could specifically cleave P_1-T/P_2 duplex from recessed 3'-termini, removing Fc to recover ECL signal.

RESULTS AND DISCUSSION

Characterization of Ag NCs-TiO_2 NFs. The Ag NCs-TiO_2 NFs was clearly seen from the TEM image (Figure 1A), where the edge portion of the TiO_2 NFs contained a large amount of Ag NCs with the average size under 2.0 nm. Meanwhile, the selected

area electron diffraction (SEAD) pattern was recorded and displayed in Figure 1B, which showed that diffraction spots were superimposed on the rings, manifesting polycrystalline structure of the nanomaterials. Then, the energy dispersive X-ray (EDX) analysis and scanning transmission electron microscopy-EDX (STEM-EDX) mapping measurements were employed to monitor the Ag content of the nanomaterials. As shown in Figure 1C, the presence of Ag (3.06 Kev) and Ti (4.49 Kev) elements verified that Ag NCs was in situ generated on TiO_2 NFs. Finally, STEM-EDX mapping measurements (Figures 1D-F) visually displayed the elemental distribution of Ag and Ti in the nanomaterials, indicating that Ag was mixed on the surface of nanomaterials, where the edge portion of the nanosphere is much than the center.

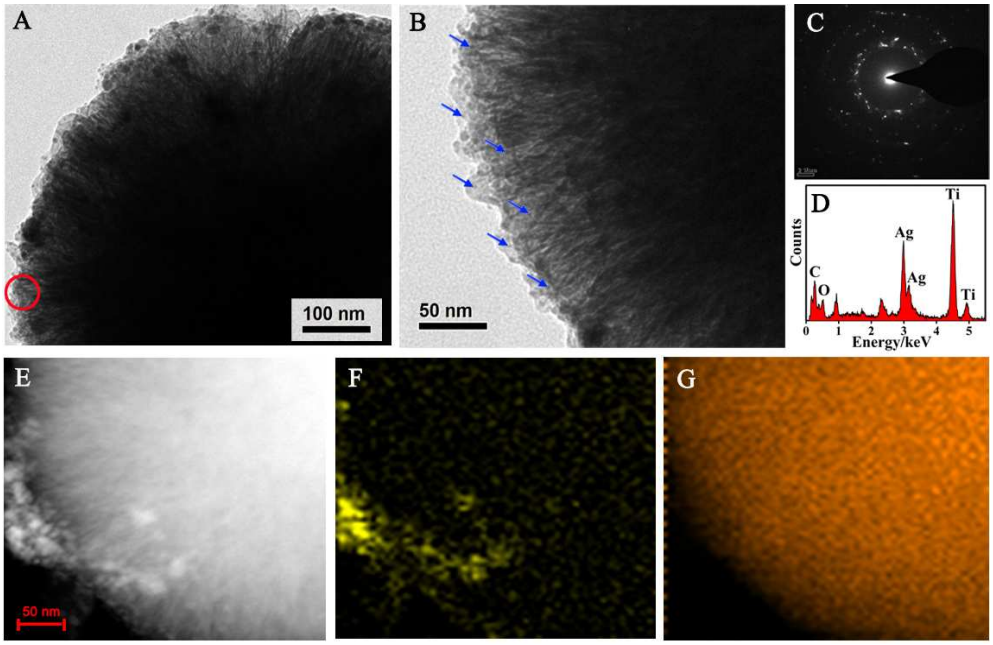

Figure 1. (A and B) magnified TEM image, (C) SEAD near the nanomaterials surface, (D) EDX element analysis and (E) STEM-HAADF image of Ag NCs-TiO_2 NFs, (F, G) STEM-EDX element mappings of Ag and Ti, respectively.

Furthermore, the photophysical characterizations of Ag NCs-TiO_2 NFs were carried out with ECL measurements, fluorescence, and UV-vis absorption spectra. The ECL

spectrum of Ag NCs-TiO_2 NFs/GCE was measured by employing optical filters, and a distinguished ECL peak at about 524 nm was observed (curve *a* of Figure 2A), which was essentially close to the fluorescence emission spectrum (493 nm, curve *b*). However, there was a 31 nm red shift of ECL emission, which indicated radical ion and triplet-triplet annihilation leading to some excimer formation [27, 28]. The UV-vis absorption spectra were employed for further researching stepwise synthetic process of the nanomaterials, and corresponding results were shown in Figure 2B. The characteristic absorption spectrum of BSA was 205.5 nm (curve *a*), while pure TiO_2 NFs had no obvious characteristic spectrum (curve *b*). Meanwhile, characteristic absorption spectrum (curve *c*) of Ag NCs-TiO_2 NFs at 216.0 nm had the red shift, attributing to quantum size effect of Ag NCs.

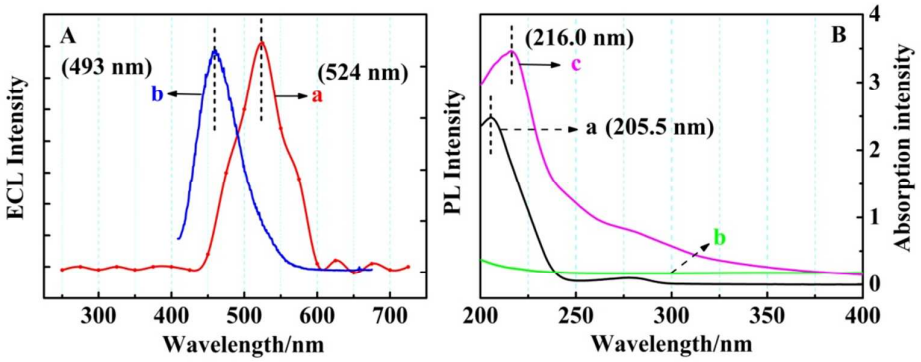

Figure 2. (A) The ECL spectrum (curve *a*) of Ag NCs-TiO_2 NFs was recorded in air-saturated PBS, and corresponding the fluorescence emission spectrum (*b*). **(B)** The UV−vis absorption spectra of BSA (*a*), TiO_2 NFs (*b*), Ag NCs-TiO_2 NFs (*c*), respectively.

Possible ECL Emitting Mechanism of Ag NCs-TiO_2 NFs. In order to demonstrate the ECL reaction mechanism of luminescent Ag NCs-TiO_2 NFs nanomaterials, relative experiments were performed. First, bare GCE and 5 μL TiO_2 NFs modified GCE (TiO_2 NFs/GCE) showed no distinct ECL emission in air-saturated PBS (Figure S3A and B). When 5 μL Ag NCs-TiO_2 NFs was dripped on GCE (Ag NCs-TiO_2 NFs/GCE), an obvious ECL response with the peak intensity

about 6665 a.u. could be seen in air-saturated PBS (Figure 3B, curve *a*), declaring that the ECL emission indeed was produced by the excited state of Ag NCs. Meanwhile, the corresponding CV showed reduction peak at -0.58 V (Figure 3A, curve *a*) due to the reduction of dissolved O_2 at the surface of the nanomaterials. And the other peak at -1.52 V suggested that the negatively charged Ag radical ($Ag\ NCs^{\bullet-}$) could directly be generated from the electro-reduction of Ag NCs by an electron injection. However, the curve *b* of Figure 3B showed a significant decline in ECL signal by immersing the Ag NCs-TiO_2 NFs/GCE in the N_2-saturated PBS containing 320 μM H_2O_2, which approximated the saturated concentration of dissolved O_2 at 25 ºC under normal atmospheric pressure. Therefore, the dissolved O_2 as the more efficient coreactant could enhance the ECL intensity of Ag NCs. After the detection solution was ventilated with highly pure N_2 for 20 min, the cathodic ECL emission conspicuously disappeared (Figure 3B, curve *c*). Furthermore, the ECL emission could be remarkably quenched (Figure 3B, curve *d*), when 0.24 mg L-cysteine was added into the 2 mL air-saturated PBS to efficiently annihilate both hydroxyl ($OH^{\bullet}$) and superoxide ($O_2^{\bullet-}$) radicals [29, 30]. Correspondingly, the CVs in the above two cases showed no distinct peaks (Figure 3A, curve *b* and *c*). When superoxide dismutase (SOD) was employed into the air-saturated solution, due to SOD as an specifical scavenger of $O_2^{\bullet-}$ [31], the ECL response showed the peak intensity about 3016 a.u (Figure 3B, curve e), indicating that the ECL emission could be promoted by $OH^{\bullet}$ species generated from the dissolved oxygen.

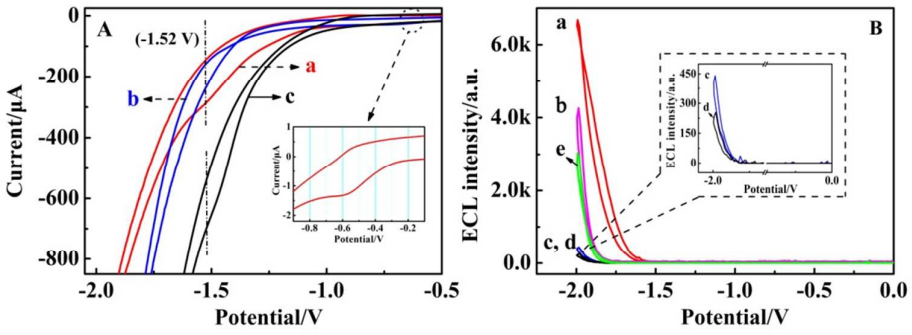

Figure 3. (A) Cyclic voltammograms of the Ag NCs-TiO_2 NFs modified GCE in air-saturated (*a*), N_2-saturated (*b*), and 1 mM L-cysteine + air-saturated (*c*) PBS. The Inset of A : magnifying CV curve *a*. **(B)** ECL-potential curves of the Ag NCs-TiO_2 NFs modified GCE in air-saturated (*a*), 320 μM H_2O_2 + N_2-saturated (*b*), N_2-saturated (*c*), 1 mM L-cysteine + air-saturated (*d*) PBS, and SOD + air-saturated (*e*) PBS. The Inset of B : magnifying ECL-potential curves *c* and *d*.

When the applied electrical energy are higher than band gap of the TiO_2 NFs, the excited electrons of valence band transit to the conduction band, generating electron-hole pairs in the surface of the TiO_2 NFs, so that accumulational O_2 on the surface of TiO_2 NFs could be reduced to form the strong oxidizing intermediate radical ($OH^{\bullet}$) (eq 1) for promoting the ECL emission of Ag NCs. While the Ag NCs underwent a reduction reaction (eq 2) to negatively charged Ag radical ($Ag^{\bullet-}$) by an electron injection, $OH^{\bullet}$ was accepted one electron from $Ag^{\bullet-}$ and transformed it to Ag* (eq 3). Finally, the Ag* excited state was generated by transferring one electron from $OH^{\bullet}$ to the LUMO of Ag, emitting intense light upon relaxation to the ground state (eq 4). The possible ECL mechanism was described as the following equations:

$$O_2 + 2H_2O + 4e^- \xrightarrow{TiO_2\ NFs} 2OH^{\bullet} + 2OH^- \quad [1]$$

$$Ag\ NCs + e^- \longrightarrow Ag\ NCs^{\bullet-} \quad [2]$$

$$OH^{\bullet} + Ag\ NCs^{\bullet-} \longrightarrow Ag\ NCs^{*} + OH^- \quad [3]$$

$$Ag\ NCs^{*} \longrightarrow Ag\ NCs + h\nu \quad [4]$$

Furthermore, the "switch off" state was obtained by incubating the ferrocene (Fc)

modified P_2 onto the electrode (Ag NCs-TiO_2 NFs/GCE), the ECL response was quenched significantly from 6665 a.u. to 541 a.u.. Upon cathodic scanning, Fc(III) was reduced to Fc(II) (eq 5), and then Fc(II) could in suit consume the dissolved O_2 (eq 6). Meanwhile, the reaction effected the electron transference and further decreased the generation of Ag* excited state. It illustrated the high-efficient quenching effect towards Ag NCs/O_2 system was observed in electron transfer path.

$$Fc(III) + e^- \longrightarrow Fc(II) \quad \text{.....[5]}$$

$$4Fc(II) + O_2 + 2H_2O \longrightarrow 4Fc(III) + 4OH^- \quad \text{.....[6]}$$

Finally, DNA T and Exo III from the output of the DNA nanostructure could trigger the release of Fc, obtaining the the second “switch on” state in the Fc-driven light switch system (Figure 4).

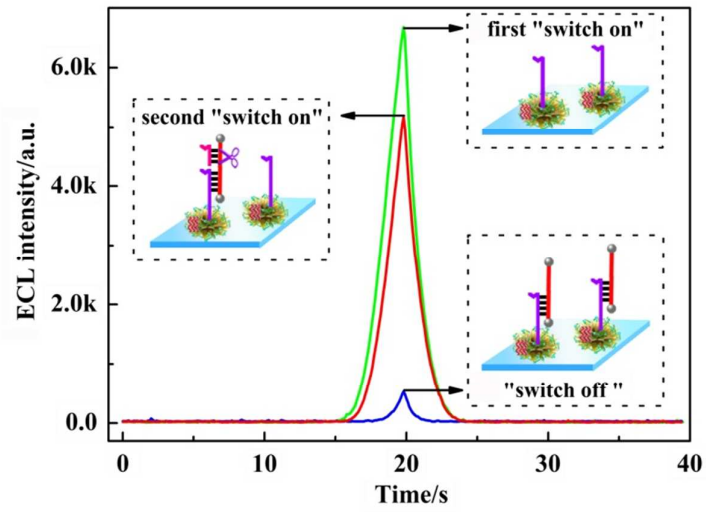

Figure 4. The schematic diagram of the Fc-driven light switch biosensor in air-saturated PBS.

Experimental Condition Optimization. In the assay, the ECL properties of Ag NCs played an important role in the performance of the biosensor. Thus the experiment condition of Ag NCs should be controlled by optimizing reaction time of Ag^+ with BSA and the concentration of Ag^+ (c_{Ag+}). Figure 5A showed different ECL intensities of the synthesized Ag NCs-TiO_2 NFs in the different reaction time of Ag^+

with BSA at 37 ºC. The ECL intensity enhanced gradually with the augment of time and then reached to a plateau after 12 h, suggesting that 12 h was enough for Ag NCs generation. Furthermore, the optimization of c_{Ag+} was carried out and a incremental ECL intensity was accordingly observed with the increase of c_{Ag+} (Figure 5B). When c_{Ag+} was greater than 5 mM, the ECL signal reached a relatively stable value owing that no more Ag NCs generated. Thus the optimized c_{Ag+} was 5 mM in the synthetic process.

On the other hand, the concentrations of Exo III ($c_{Exo\ III}$) was of great significance, which because it directly influenced the quantitative determination of bisensor. As shown in Figure 5C, a consecutive increased ECL intensity was observed when concentration at the range of 10 to 30 U mL^{-1}. And then a plateau was reached at 30 U mL^{-1}, thus the optimized $c_{Exo\ III}$ was 30 U mL^{-1} in the work.

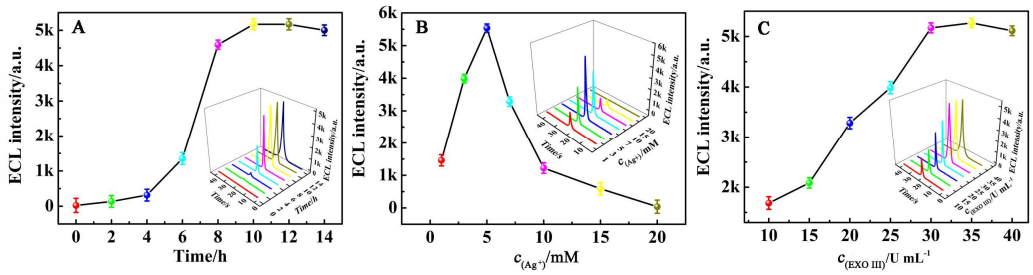

Figure 5. (A) Optimum reaction time of Ag^+ with BSA at 37 ºC; (B) Optimum concentration of Ag^+; (C) Optimum concentration of Exo III. All the ECL intensity was detected in air-saturated PBS (pH 7.4).

Detection of Aβ with the Proposed Biosensor. After incubation with different concentrations of the preceding released T for 2 h, the developed biosensor was measured in air-saturated PBS to evaluate the detection sensitivity of Aβ under the optimized experimental conditions. From Figure 6A, the ECL signal obviously increased with an increase in the concentration of Aβ (curves a~h) presented an excellent linear relationship with the logarithm of concentration. The linear equation

was ΔI = 667.0 lg $c_{A\beta}$+ 2967 with the correlation coefficient square of 0.9955, where ΔI was the change of ECL intensity ($I_{\text{second "switch on"}}$ - $I_{\text{"switch off"}}$) and $c_{A\beta}$ was the concentration of Aβ. Additionally, the estimated limit of detection (LOD) was 32 fg mL^{-1} (the detailed calculation process presented in Supporting Information). Previous researchs about protein detection based metal NCs was used to have a comparative study, in which the proposed biosensors exhibited better sensitivity comparing with previously researches (Table 1).

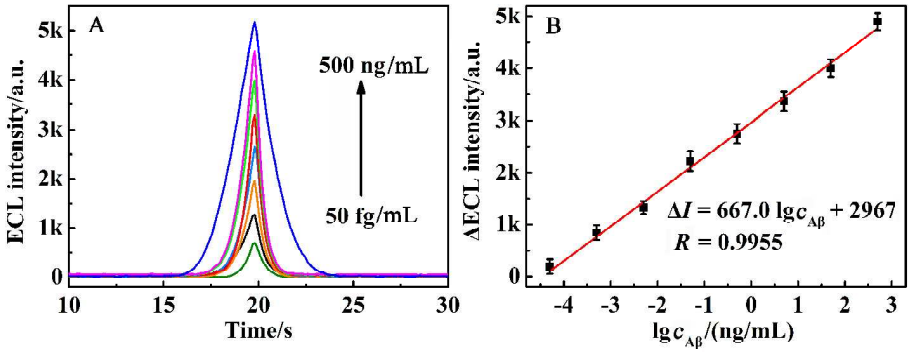

Figure 6. (A) ECL profiles of the biosensor incubating Aβ with different concentrations: 50 fg mL^{-1}, 500 fg mL^{-1}, 5 pg mL^{-1}, 50 pg mL^{-1}, 500 pg mL^{-1}, 5 ng mL^{-1}, 50 ng mL^{-1}, and 500 ng mL^{-1}. (B) Calibration plots of the proposed biosensor.

Table 1. Comparison of the This Work with the Previous Researchs.

methods	signal probe	target	detection limit	references
fluorescence	Au NCs	human α -thrombin	36.7 μg mL^{-1}	32
fluorescence	Au NCs	histone deacetylase 1	175 ng mL^{-1}	33
electrochemistry	Ag NCs	alpha-fetoprotein	0.8 pg mL^{-1}	34
photoelectrochemistry	Ag NCs	carcinoembryonic antigen	1.0 pg mL^{-1}	35
ECL	Pd NCs	carcinoembryonic antigen	0.62 pg mL^{-1}	36
ECL	Ag NCs	amyloid-β (Aβ)	32 fg mL^{-1}	this work

Performance of the Proposed Biosensor. The stability of this proposed biosensor with different concentrations of Aβ was assessed by continuous cyclic scans. As shown in Figure 7A, with the increase of Aβ concentrations, the ECL intensities

increased and the scanning curves were relative stable under three consecutive cycles at every concentration. Susequently, the selectivity of the ECL biosensor for Aβ was demonstrated by opposing other interferences of apolipoprotein-A1 (Apo-A1) immunoglobulin G (IgG) and hexanethiol (HT). From the results in Figure 7B, it could be seen that the ECL intensities of Apo-A1 (50 ng mL^{-1}), IgG (50 ng mL^{-1}) and HT (50 ng mL^{-1}) significantly decreased comparing with that of the interference experiment at the presence of Aβ (500 pg mL^{-1}). Furthermore, the ECL intensity of the biosensor with a mixture solution (500 pg mL^{-1} Aβ containing 50 ng mL^{-1} Apo-A1, 50 ng mL^{-1} IgG, 50 ng mL^{-1} HT) was approached to that incubating with 500 pg mL^{-1} Aβ. Such high selectivity could be attributed to combination the good specific immune recognition of immunoreaction with the exquisite sequence specificity of double-stranded DNA. Therefore, the assay approach had perfect stability, precision, and accuracy, showing potential applications in clinical diagnostics (the clinical serum samples analysis showed in Table S2).

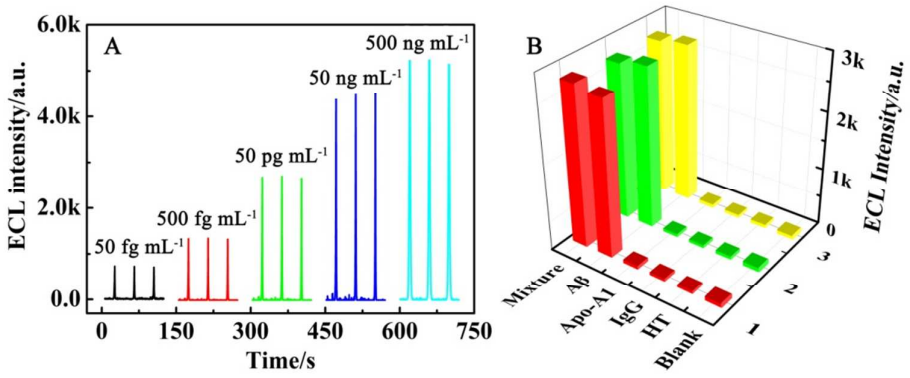

Figure 7. (A) The ECL stability of the proposed biosensor to various concentrations of Aβ. (B) Selectivity of the biosensor detection of Aβ (500 pg mL^{-1}) against the interference proteins: 50 ng mL^{-1} Apo-A1, 50 ng mL^{-1} IgG, and 50 ng mL^{-1} HT.

CONCLUSION

Highly efficient ECL of a novel Ag NCs-TiO_2 NFs nanomaterials, which combined TiO_2 NFs as the co-reaction accelerator with intrinsic O_2 as the co-reactant during the

ECL emission process of Ag NCs, was observed for the first time. Meanwhile, the Ag NCs-TiO_2 NFs had numerous advantages, such as great biocompatibility, ease of labeling and easy film-forming, which provided a facile platform for integrating Fc-driven light switch system and immunoreaction-induced DNA nanostructure for ultrasensitive detection of Aβ. In view of these advantages, the nanomaterials had great potential as a high-performance NCs-based platform in ultrasensitive bioanalysis.

ASSOCIATED CONTENT

Supporting Information

Reagents and apparatus, SDS-PAGE analysis, preparation of 16 nm-AuNPs, ECL response curves of bare GCE and TiO_2 NFs modifying GCE, mechanism of the target Aβ conversion, characterization of the stepwise fabrication, reproducibility, limit of detection calculation, and application of the immunosensor are provided as Supporting Information. This material is available free of charge via the Internet at http://pubs.acs.org.

AUTHOR INFORMATION

* Corresponding authors

Tel.: +86 23 68252277, fax: +86 23 68253172.

E-mail addresses: yuanruo@swu.edu.cn (R. Yuan), yqchai@swu.edu.cn (Y. Q. Chai).

Notes

The authors declare no competing financial interest.

ACKNOWLEDGMENT

This work was financially supported by the National Natural Science Foundation (NNSF) of China (Grants 51473136, 21575116, and 21675129), China Postdoctoral Science Foundation (2016M602626) and the Fundamental Research Funds for the Central Universities (Grant XDJK2015A002, XDJK2014A012), China.

REFERENCES

(1) Hesari, M.; Workentin, M. S.; Ding, Z. *ACS Nano* **2014**, 8, 8543-8553.

(2) Hesari, M.; Workentin, M. S.; Ding, Z. *Chem. Sci.* **2014**, 5, 3814-3822.

(3) Tian, R.; Zhang, S.; Li, M.; Zhou, Y.; Lu, B.; Yan, D.; Wei, M.; Evans, D. G.; Duan, X. *Adv. Funct. Mater.* **2015**, 25, 5006-5015.

(4) Chen, T.; Hu, Y.; Cen, Y.; Chu, X.; Lu, Y. *J. Am. Chem. Soc.* **2013**, 135, 11595-11602.

(5) Han, G. M.; Jia, Z. Z.; Zhu, Y. J.; Jiao, J. J.; Kong, D. M.; Feng, X. Z. *Anal. Chem.* **2016**, 88, 10800-10804.

(6) Zhang, L.; Wang, E. *Nano Today* **2014**, 1, 132-157.

(7) Swanick, K. N.; Hesari, M.; Workentin, M. S.; Ding, Z. *J. Am. Chem. Soc.* **2012**, 134, 15205-15208.

(8) Li, L.; Liu, H.; Shen, Y.; Zhang, J.; Zhu, J. J. *Anal. Chem.* **2011**, 83, 661-665.

(9) Chen, A. Y.; Ma, S.; Zhuo, Y.; Chai, Y. Q.; Yuan, R. *Anal. Chem.* **2016**, 88, 3203-3210.

(10) Chen, T.; Hu, Y.; Cen, Y.; Chu, X.; Lu, Y. *J. Am. Chem. Soc.* **2013**, 135, 11595-11602.

(11) Miller, E. W.; Tulyanthan, O. E.; Isaciff, Y.; Chang, C. J. Nat. *Chem. Biol.* **2007**, 3, 263-267.

(12) Chen, Z.; Liu, Z.; Li, Z.; Ju, E.; Gao, N.; Zhou, L.; Ren, J.; Qu, X. *Biomaterials* **2015**, 39, 15-22.

(13) Kumar, S.; Rhim, W. K.; Lim, D. K. Nam, J. M. *ACS NANO* **2013**, 3, 2221-2230.

(14) Bourikas, K.; Kordulis, C.; Lycourghiotis, A. *Chem. Rev.* **2014**, 114, 9754-9823.

(15) Liu, L.; Ouyang, S.; Ye, J. *Angew. Chem. Int. Ed.* **2013**, 52, 6689-6693.

(16) Xie, J.; Zheng, Y.; Jackie, Y.; Ying, *J. Am. Chem. Soc.* **2009**, 131, 888-889.

(17) Cao, L.; Zhang, R.; Zhang, W.; Du, Z.; Liu, C.; Ye, Z.; Song, B.; Yuan, J. *Biomaterials* **2015** 68, 21-31.

(18) Li, F.; Yu, Y.; Li, Q.; Zhou, M.; Cui, H. *Anal. Chem.* **2015**, 87, 7787-7794.

(19) Kingsmore, S. F. *Nat. Rev. Drug. Discov.* **2006,** 5, 310-321.

(20) Aponte, J. J.; Aide, P.; Renom, M.; Mandomando, I.; Bassat, Q.; Sacarlal, J.; Manaca, M. N.; Lafuente, S. *Lancet* **2007**, 370, 1543-1551.

(21) Zhang, H.; Lai, M.; Zuehlke, A.; Peng, H.; Li, X. F.; Le, X. C. *Angew. Chem. Int. Ed.* **2015**, 127, 14534-14538.

(22) Button, K. S.; Ioannidis, J. P. A.; Mokrysz1, C.; Nosek, B. A.; Flint, J.; Robinson, E. S. J.; Munafò, M. R. *Nat. Rev.* **2013**, 14, 365-376.

(23) Villemagne, V. L.; Burnham, S.; Bourgeat, P.; Brown, B. *Lancet* **2013**, 13, 70044-70049.

(24) Xiong, E.; Zhang, X.; Liu, Y.; Zhou, J.; Yu, P.; Li, X.; Chen, J. *Anal. Chem.* **2015**, 87, 7291-7296.

(25) Liu, X.; Wang, F.; Aizen, R.; Yehezkeli, O.; Willner, I. *J. Am. Chem. Soc.* **2013**, 135, 11832-11839.

(26) Fan, D.; Zhu, X.; Zhai, Q.; Wang, E.; Dong, S. *Anal. Chem.* **2016**, 88, 9158-9165.

(27) Liang, W.; Zhuo, Y.; Xiong, C.; Zheng, Y.; Chai, Y. Q.; Yuan, R. *Anal. Chem.* **2015**, 87, 12363-12371.

(28) Kim, J. H.; Kim, J. H. *J. Am. Chem. Soc.* **2012**, 134, 17478-17481.

(29) Deng, S. Y.; Hou, Z. T.; Lei, J. P.; Lin, D. J.; Hu, Z.; Yan, F.; Ju, H. X. *Chem. Commun.* **2011**, 47, 2107-12109.

(30) Jiang, H.; Ju, H. X. *Anal. Chem.* **2007**, 79, 6690-6696.

(31) Nistri, S.; Boccalini, G.; Bencini, A.; Becatti, M.; Valtancoli, B.; Conti, L.; Lucarini, L.; Bani, D. *Free Radic. Res.* **2015**, 49, 67-77.

(32) Li, J.; Zhong, X.; Zhang, H.; Le, X. C.; Zhu, J. J. *Anal. Chem.* **2012**, 84, 5170-5174.

(33) Wen, Q.; Gu, Y.; Tang, L. J.; Yu, R. Q.; Jiang, J. H. *Anal. Chem.* **2013**, 85, 11681-11685.

(34) Zhang, B.; Liu, B.; Zhou, J.; Tang, J.; Tang, D. P. *ACS Appl. Mater. Interfaces* **2013**, 5, 4479-4485.

(35) Song, J.; Wang, J.; Wang, X.; Zhao, W.; Zhao, Y.; Wu, S.; Gao, Z.; Yuan, J.; Meng, C. *Biosens. Bioelectron.* **2016**, 80, 614-620.

(36) Huang, Y.; Lei, J.; Cheng, Y.; Ju, H. X. *Biosens. Bioelectron.* **2016**, 77, 733-739.

For TOC only

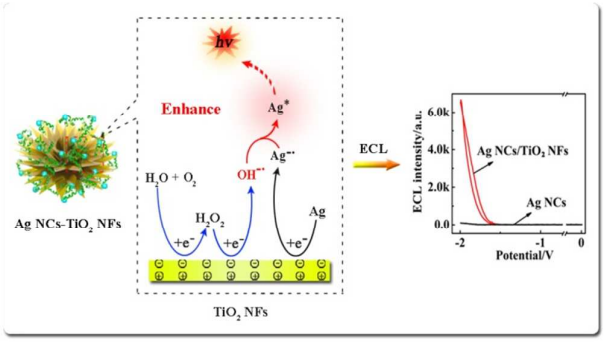
hv
Enhance
Ag*
Ag**
OH**
H2O + O2
H2O2
Ag
+e-
+e-
+e-
Ag NCs-TiO2 NFs
TiO2 NFs
ECL
ECL intensity/a.u.
6.0k
4.0k
2.0k
0.0
Ag NCs/TiO2 NFs
Ag NCs
-2
-1
0
Potential/V